

An Improved Programmable Grating Array Based Wavefront Sensor

Biswajit Pathak^a

^aDepartment of Engineering Science, University of Oxford, Parks Road, Oxford OX1 3PJ, UK

ABSTRACT

An improved programmable grating array based wavefront sensor (GAWS) is proposed which is capable of estimating the incident wavefront more accurately, by generating an array of uniform intensity +1 order spots with negligible contribution from unwanted higher order spots. The duty cycle of each grating element of the proposed sensor is effectively varied in order to independently control the intensity of each +1 order spot. Furthermore, random binarisation technique is implemented on the diffraction grating array to reduce the contribution from undesirable higher order spots by disintegrating them into noise. Proof-of-principle simulation results are presented to demonstrate the working of the proposed GAWS in comparison to the conventional GAWS, for non-uniform intensity of the +1 order spots.

Keywords: Shack-Hartmann Wavefront Sensor, Diffraction Grating, Centroid, Wavefront Estimation

1. INTRODUCTION

The Shack Hartmann wavefront sensor (SHWS) is one of the most popular zonal wavefront sensors that consists of a 2D array of lenslets and a camera which is placed at the common focal plane of the lenslets. It is observed that when an unaberrated wavefront is incident on the lenslets array, a uniform pattern of spots is generated on the focal plane of the lenslets array which are commonly referred to as reference spots. However, the presence of distortion in the incident wavefront displaces the focal spots from their original positions by an amount proportional to the tilt of the wavefront across its lenslets aperture. The amount of displacement between the reference and displaced focal spot centroid positions contain vital information about the local wavefront slopes of the incident wavefront which is then used in a zonal or modal wavefront estimation algorithm¹⁻³ to generate the phase profile of the incident wavefront. Another variant of zonal wavefront sensor is the programmable grating array based wavefront sensor (GAWS) which is constructed by replacing the lenslets array present in the SHWS with an array of 2D plane diffraction gratings (implemented using a spatial light modulator) together with a single focusing lens.^{4,5} When the grating array of the GAWS is illuminated with a collimated laser beam, then a number of diffracted orders such as ± 1 , ± 3 , ± 5 , etc., are generated. However, only the +1 orders are chosen from each grating element amongst all the diffracted orders owing to its high intensity to result in a regular 2D array of focal spots in the camera plane for an unaberrated incident wavefront. The working principle of the GAWS is similar to that of the SHWS with a number of advantages due to its programmable nature, such as flexibility in the camera geometry,^{6,7} enhanced spatial resolution⁸ and improved wavefront estimation accuracy.⁹ However, in the conventional design, the fixed intensity of the +1 order spots and the presence of undesirable higher order spots that adversely affect the centroid calculation are counted as some of its important limitations.

The accurate calculation of the focal spot centroid position is extremely important for accurate estimation of the wavefront slope^{10,11} as otherwise, the error due to inaccurate centroid calculation propagates through the estimation algorithm to result in an inaccurate wavefront estimation.^{3,12} It is noteworthy that if the intensity of focal spots in a zonal wavefront sensor is either faint or saturated then it leads to erroneous centroid calculation.¹³ In other words, the signal-to-noise ratio (SNR) of the focal spots will not be uniform to calculate each centroid position with enough accuracy. The centroid of focal spots with low SNR is generally not measured. As a result, it leads to loss of information. Now, to compensate for the centroid information from these unmeasured (low SNR) focal spots, the estimated wavefront is extrapolated which incorporates an additional error.¹⁴ In order to

Further author information: (Send correspondence to B.P.)

B.P.: E-mail: biswajit.pathak@eng.ox.ac.uk

obtain an array of focal spots with equivalent SNR, a sequence of focal spot images with different exposure times of the camera is captured.¹³ For instance, a camera with readout speed of F frames per second will require a minimum of $\frac{N}{F}$ seconds to capture N number of frames with different exposure times of the camera. Thus, the use of multiple camera frames makes the process complex and time consuming. The intensity of the focal spots (or +1 order spots) in a zonal wavefront sensor may not be uniform in a number of practical cases¹⁵ such as ophthalmic wavefront sensing,^{16,17} transmitted light in an optical fibre,¹⁵ unevenly coated optical elements,¹⁸ thin film measurement arrangement.¹⁹ It is to be mentioned that non-uniform +1 order spot intensities in a GAWS will affect the centroid calculation more severely than the focal spots in SHWS. This is due to the fact that presence of unwanted higher order spots in GAWS will either contribute to the centroid calculation of the +1 order spots, or their contribution will be removed along with the necessary +1 order spots, when applying a threshold value to remove the higher order spots. Figure 1 illustrates the problem associated with a conventional GAWS for a particular situation when the array of +1 order spots have non-uniform intensities and contain unwanted higher order spots which are detrimental to centroid calculation process.

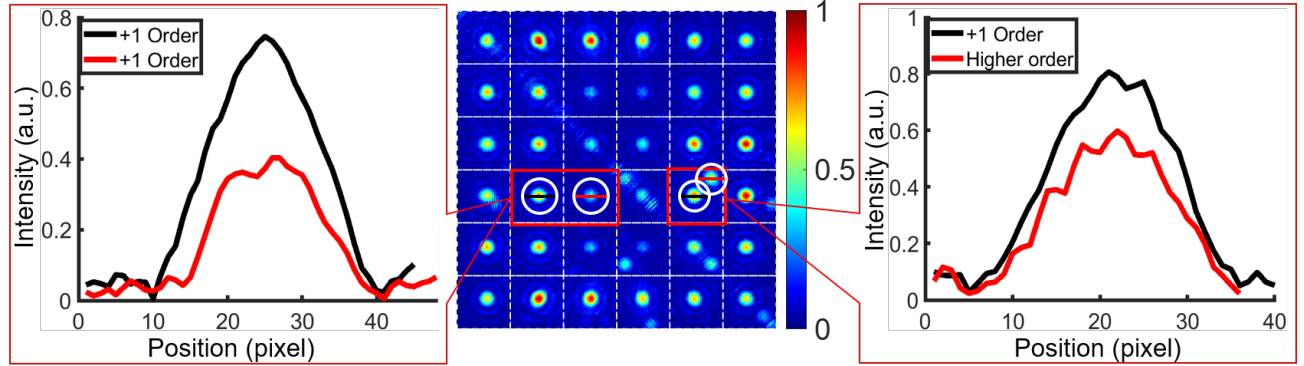


Figure 1. Illustration of an array of +1 order spots that has non-uniform intensities and presence of unwanted higher order spots.

In the present work, an improved GAWS is proposed that uniformises the variation in intensity of the array of +1 order spots with negligible contribution from unwanted higher order spots. The duty cycle of each grating element of the proposed sensor can be effectively varied in order to independently control the intensity of each +1 order spot. Furthermore, random binarisation technique is implemented on the diffraction grating array to reduce the contribution from undesirable higher order spots by disintegrating them into noise. Proof-of-principle simulation results are presented to demonstrate the working of the proposed GAWS in comparison to the conventional GAWS, for non-uniform intensity of the +1 order spots.

2. METHODOLOGY

In the proposed GAWS,²⁰ the intensity of the +1 order spots can be manipulated by changing the width of the transmittance portion of the diffraction grating, which is also known as the duty cycle (details about the construction of the conventional GAWS can be found elsewhere^{4,5}). The duty cycle of a binary diffraction pattern is defined as the ratio of the opaque or transmittance width (t) to the period of the grating pattern (p), i.e., $D = \frac{t}{p}$. The efficiency of the +1 order spot as a function of the duty cycle and the order number n ²¹ is given by Eq. 1 as shown below,

$$\beta = \left(\frac{t}{p}\right)^2 \times \text{sinc}^2\left(\frac{nt}{p}\right). \quad (1)$$

We define the transmittance function of the array of binary diffraction gratings with variable duty cycle, as given below

$$T_G(x, y) \Big|_{(i,j)=(1,1)}^{(i,j)=(N,N)} = \begin{cases} 1 & \text{if } \cos [\phi^{i,j}(x, y) + (m_{0x}^i x + m_{0y}^i y)] \geq \sqrt{1 - I_{i,j}^2} \\ 0 & \text{if } \cos [\phi^{i,j}(x, y) + (m_{0x}^i x + m_{0y}^i y)] < \sqrt{1 - I_{i,j}^2} \end{cases} \quad (2)$$

where $\phi(x, y)$ represents the user defined phase function that can be expressed as a linear combination of an orthogonal basis function, such as Zernike polynomials²² (here $\phi^{i,j}(x, y) = 0$ for each grating element) and $I_{i,j}$ represents the desired intensity of the +1 order spot corresponding to the $(i, j)^{th}$ grating element such that a minimum and maximum intensity of the +1 order spot can be either 0 or 1, respectively. The amount of deflection of the desired order with respect to the undiffracted zero order is represented by (m_{0x}^i, m_{0y}^i) , given as

$$\begin{aligned} m_{0x}^i &= m_{0x}^1 + (i - 1) \times \Delta m_{0x} \\ m_{0y}^j &= m_{0y}^1 + (j - 1) \times \Delta m_{0y}. \end{aligned} \quad (3)$$

Here, (m_{0x}^1, m_{0y}^1) is the spatial frequency of the top left grating element (i.e., 1,1) and $(\Delta m_{0x}, \Delta m_{0y})$ are real numbers that apply a uniform increment between the adjacent grating elements along i (row index) and along j (column index).

Using Eq. 2 we can vary the duty cycle of any of the grating element to obtain a desired intensity of the +1 order spots.^{21,23} Thus, we can independently control the intensity of each +1 order spot so that the intensity of the entire array of +1 orders can be uniformised.

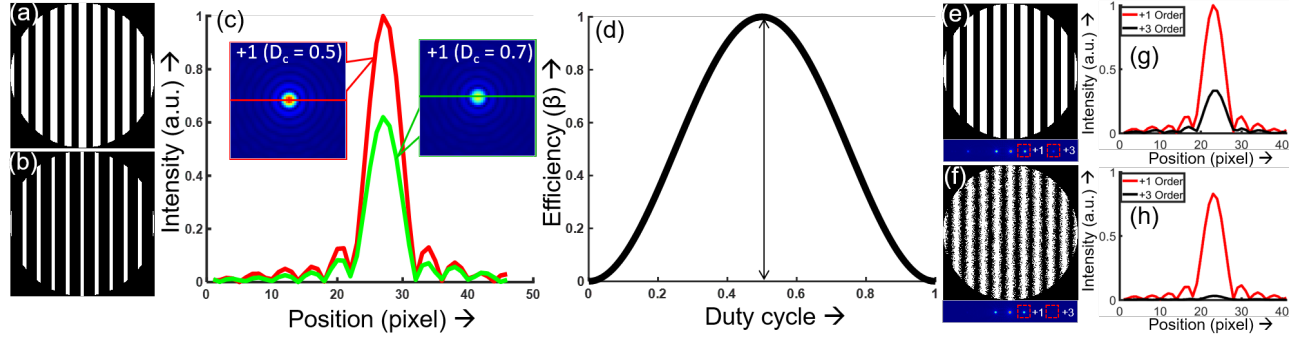


Figure 2. A binary diffraction grating element with (a) $D = 0.5$ and (b) $D = 0.7$ and the corresponding line plots across the center of +1 order spot for $D = 0.5$ (red solid line) and $D = 0.7$ (green solid line) are shown in (c). The diffraction efficiency plot of the +1 order spot as a function of duty cycle is illustrated in (d). The binary diffracting grating element (e) before implementation of random binarisation ($q = 0$) and (f) after implementation of random binarisation ($q = 0.8$) and its corresponding line plots across the center of +1 order spot and the +3 order spot (higher order) are shown in (g) and (h), respectively (diffracted spots are shown at the bottom of (e) and (f), respectively).

The centroid calculation of +1 order spots using GAWS is erroneous in presence of higher order spots which can be tackled by implementing random binarisation to the diffraction grating array such that the higher order spots can be reduced to noise.^{24,25} This can be achieved by following the mathematical relation, given by Eq. 4 as expressed below,

$$T_R(i, j) = \begin{cases} 1 & \text{if } T_G^{i,j}(x, y) \geq qr(x, y) \\ 0 & \text{if } T_G^{i,j}(x, y) < qr(x, y) \end{cases} \quad (4)$$

where r represents a uniform distribution of random numbers between 0 and 1, and q is a real number with values ranging between 0 and 1 which can be used to scale the amplitude of randomisation to reduce the

effect from higher order spots. Figure 2 illustrates the manipulation of +1 order spots intensity by varying the duty cycle of a single grating element independently and reducing the contribution of higher order spots by implementing random binarisation of the grating element. Figure 2(a) and Fig. 2(b) represents the binary diffraction grating element with $D = 0.5$ and $D = 0.7$ and the respective line plots corresponding to the center of +1 order spots are shown in Fig. 2(c). The line plot in Fig. 2(d) represents the variation of diffraction efficiency (β) as a function of the duty cycle (D) for the first order spot ($n = +1$). It is observed from the plot that the diffraction efficiency gives a maximum value for $D = 0.5$ and minimum values for $D = 0$ and $D = 1$. Figure 2(e) and Fig. 2(f) represents the binary diffracting grating element with $q = 0$ and $q = 0.8$, respectively and the corresponding line plots across the center of +1 order spot and the +3 order spot (higher order) are shown in Fig. 2(g) and Fig. 2(h), respectively.

It is evident that the intensity of higher order spots (i.e., $n > \pm 1$) reduces significantly for $q = 0.8$ after implementation of random binarisation in comparison to $q = 0$, before implementation of random binarisation. Noteworthy, that randomisation may introduce some random background noise as well as reduce the intensity of the +1 order spots by a small amount. The former can be eliminated by putting a threshold value whereas the latter can be neglected as the decrease in intensity is very small (i.e., $\frac{1}{n^2\pi^2}$) in comparison to the decrease observed in the case of higher order spots ($n = \pm 3, \pm 5$, etc), so it does not pose a significant issue. Thus, the intensity of the desired +1 order spots can be manipulated and the diffraction effect from higher order spots can be reduced using Eq. 2 and Eq. 4 consecutively. It is to be noted that to implement the proposed GAWS, prior information on the intensity of the array of +1 order spots and the maximum intensity of the higher order spots present is required, corresponding to a fixed duty cycle of the binary diffraction grating array (as in the case of conventional GAWS). Based on these intensity information, the duty cycle of the binary diffraction grating array is manipulated using Eq. 2 and random binarisation is implemented using Eq. 4 consecutively, to uniformise the intensity and minimise the higher order diffraction effects from the same array of +1 orders spots.

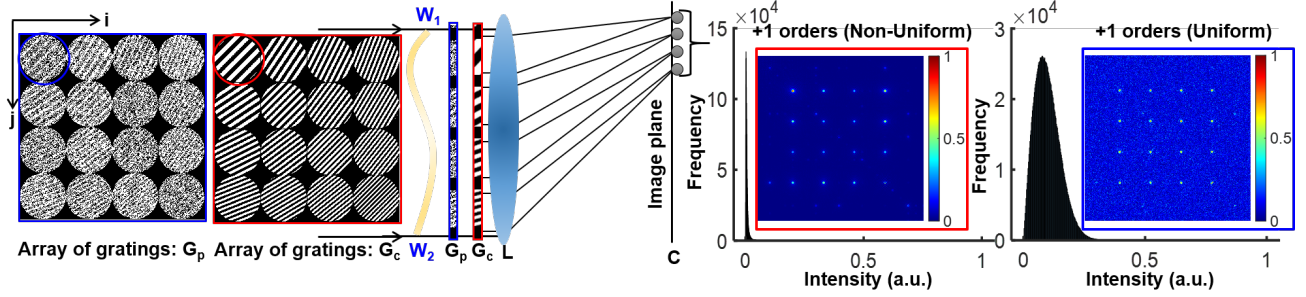


Figure 3. Schematic diagram of the conventional and proposed GAWS. The transmittance profile of the conventional grating array G_c and the corresponding +1 order spots are shown within the red solid boxes (array of +1 order spots is shown in the inset of its histogram plot), whereas the transmittance profile of the proposed grating array G_p and the corresponding +1 order spots are shown within the blue solid boxes (array of +1 order spots is shown in the inset of its histogram plot), respectively.

Figure 3 represents a schematic diagram of the conventional as well as proposed GAWS. A collimated light beam incident on the 2D binary grating array gets diffracted and is finally focused by lens L onto the image plane where a camera C is placed. The transmittance function of the 2D grating array G_c corresponding to the conventional GAWS is configured using an equation similar to Eq. 2, with the term $\sqrt{1 - I_{i,j}^2}$ replaced by 0, to form a regular 2D array of focal spots in the case of unaberrated incident wavefront. When an incident wavefront with non-uniform illumination intensity profile such as W_1W_2 , is considered, then it results in +1 order spots with non-uniform intensity together with a number of higher order spots in the image plane (shown within the red solid box in the inset of its histogram plot). The higher order spots are generally eliminated by putting a threshold. In such a situation, considering an appropriate threshold value is critical as any in-appropriate value will either eliminate contribution from necessary +1 order spots or will incorporate contribution from unwanted higher order spots. This severe issue can be effectively addressed by considering the proposed GAWS where the transmittance function of the 2D grating array G_p is constructed using Eq. 2 and Eq. 4 consecutively. This

results in an array of uniform intensity +1 order spots with negligible contribution from higher order spots (as shown within the blue solid box in the inset of its histogram plot).

3. RESULTS AND DISCUSSION

The working of both the conventional and proposed GAWS has been illustrated through simulation results. For the purpose, we consider a beam with Gaussian intensity distribution profile and vary its diameter and position, relative to the center of the grating array to generate an array of +1 order spots with variation in their intensities. The transmittance function of the binary grating array, having a dimension of 6×6 was defined according to Eq. 2, and then Fourier Transform operation was performed to generate the 2D array of +1 order spots (the numerical simulations were performed in MATLAB R2015b version). The relationship between β and D is used to vary the duty cycle of the diffraction grating (G_p) so that the intensity of all the spots in the array becomes equivalent. This is followed by implementation of random binarisation of the diffraction grating array according to Eq. 4, in order to eliminate the effect of higher order spots. Figure 4(i) represents the array of uniform intensity +1 order spots obtained using the conventional GAWS, corresponding to a centered Gaussian illumination intensity profile with a larger beam diameter that overfills the grating array (so as to have a uniform intensity across the grating array dimension of 6×6). Similarly, Fig. 4(ii) and Fig. 4(iv) represents the array of non-uniform intensity +1 order spots using the conventional GAWS, corresponding to centered and off-centered Gaussian illumination intensity profiles with a beam diameter equivalent to that of the grating array dimension. Figure 4(iii) and Fig. 4(v) represents the array of +1 order spots whose intensity has been uniformised and higher order spots have been minimised using the proposed GAWS, corresponding to the illumination profiles considered in Fig. 4(ii) and Fig. 4(iv), respectively. These simulation results clearly show that the proposed GAWS generates an array of uniform intensity +1 order spots as well as eliminates the undesirable effects from higher order spots. It is observed that in Fig. 4(iii) and Fig. 4(v), there is presence of uniformly distributed small random noise arising from the breakdown of the higher order spots which can now be easily eliminated by putting a threshold value.

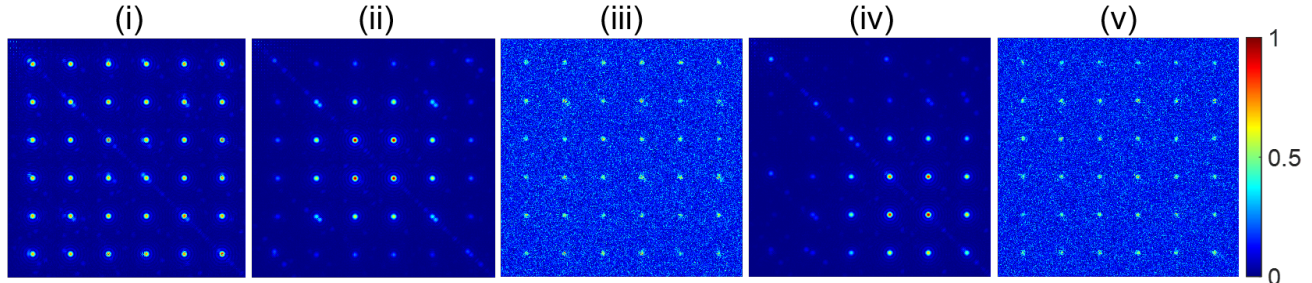


Figure 4. The 2D array of +1 order spots (obtained using conventional GAWS) with (i) uniform intensity corresponding to a centered Gaussian illumination intensity profile having a larger beam diameter that overfills the grating array. The 2D array of +1 order spots with (ii) non-uniform and (iii) uniform intensities obtained using the conventional GAWS and proposed GAWS, respectively, corresponding to a centered Gaussian illumination intensity profile. Similarly, the 2D array of +1 order spots with (iv) non-uniform and (v) uniform intensities obtained using the conventional GAWS and proposed GAWS, respectively, corresponding to off-centered Gaussian illumination intensity profiles. The intensity values have been normalised in between 0 and 1 and a common bar plot is shown at the extreme right.

Another set of simulation result has been presented to demonstrate the wavefront estimation accuracy using the proposed GAWS in comparison to the conventional GAWS. Implementing computer generated holography technique,^{26,27} it is possible to generate +1 order beams with phase profiles corresponding to user defined monochromatic aberrations. We use the phase function $\phi(x, y)$ to represent a beam with classical aberrations expressed as a linear combination of single indexed Zernike polynomials,²² such that $\phi(x, y) = \sum a_j Z_j(x, y)$ (where a_j represents the root mean square amplitudes of the j^{th} mode in radians and now $\phi(x, y)$ is defined with the same dimension as the total grating array dimension). The centroid position is measured initially without applying the phase profile (reference spots) and then with the applied phase $\phi(x, y)$ added holographically (shifted spots) by using the standard center of mass algorithm¹¹ of each +1 order spots. The focal spot shifts obtained from

both the images are used to calculate the horizontal and vertical slopes from which the incident wavefront can be estimated. Figure 5 shows the applied and estimated phase profiles for both conventional and proposed GAWS using the modal wavefront estimation¹ method (considering Zernike modes $Z_4 \rightarrow Z_{24}$) for centered as well as off-centered Gaussian illumination intensity profiles for a grating array dimension of 6×6 . Figure 5(i)(a) shows the applied phase profile for $\phi(x, y) = 0.3Z_5 - 0.8Z_8 + 0.6Z_{10} - 0.4Z_{11}$. The bar diagram in Fig. 5(i)(b) represent the RMS amplitudes of the Zernike modes detected in the case of centered Gaussian illumination intensity profile with a larger beam diameter that overfills the grating array, using the conventional GAWS. The bar diagrams in Fig. 5(ii)(a) and Fig. 5(iii)(a) represents the RMS amplitude of the Zernike modes detected in the case of centered Gaussian using the conventional and proposed GAWS, respectively. Similarly, the RMS amplitudes of the Zernike modes detected in the case of off-centered Gaussian using the conventional and proposed GAWS are shown in bar diagram plots of Fig. 5(ii)(b) and Fig. 5(iii)(b), respectively. All the plots in Fig. 5 are in radian units and the estimated phase profile using the detected Zernike mode amplitudes are shown within the inset of the respective bar plots. The value of RMS error calculated from the difference between applied and estimated phase profiles is found to be 0.0784 radian for centered Gaussian illumination intensity profile (for beam diameter that overfills the grating array) using the conventional GAWS (a threshold value was considered here). Similarly, the value of RMS errors are found to be 0.2636 radian and 0.3385 radian for centered Gaussian and off-centered Gaussian intensity profiles using the conventional GAWS whereas the same in the proposed GAWS are found to be 0.1050 radian and 0.1216 radian, respectively. The results show that the RMS errors are smaller for the proposed GAWS in comparison to the conventional GAWS for non-uniform intensity of the +1 order spots, and it is also close to the value when the +1 order spots are of uniform intensity, in the case of conventional GAWS. This reduction in RMS error is due to the fact that centroid calculation error is quite smaller when the focal spot intensities are uniform and the magnitude of the higher order spots is small.

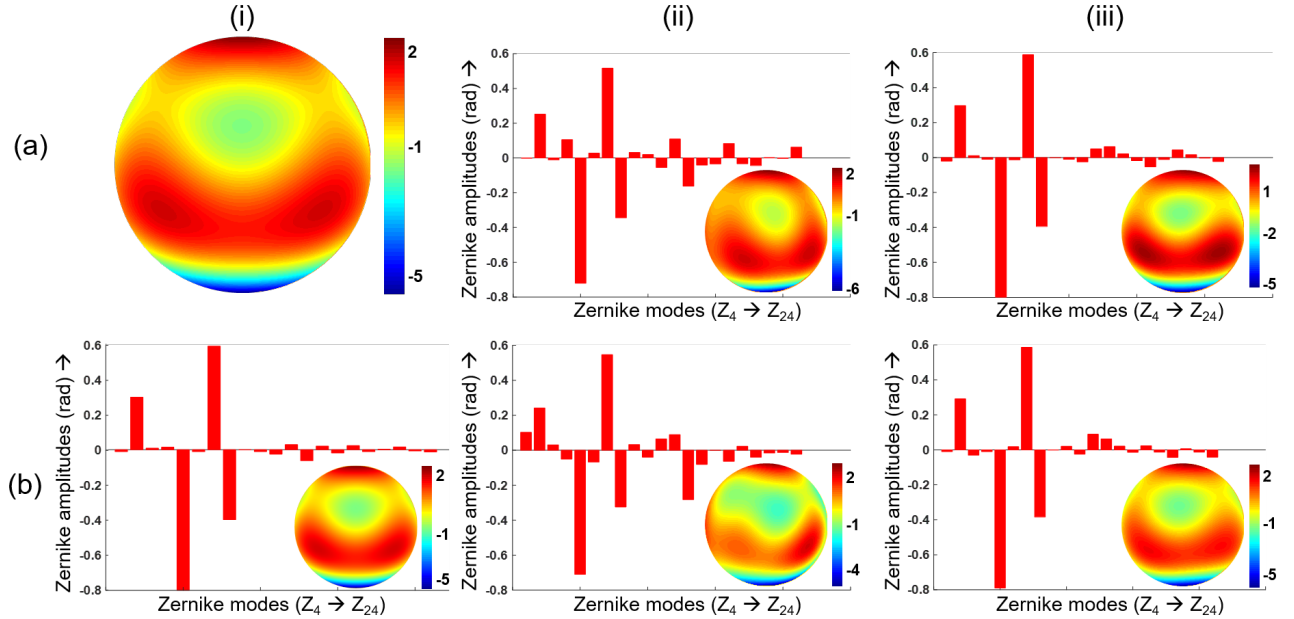


Figure 5. False color images representing the (i)(a) applied phase profile and its corresponding (i)(b) bar diagram plot showing the RMS amplitudes of the Zernike modes detected in the case of centered Gaussian illumination intensity profile (beam diameter that overfills the grating array), using the conventional GAWS. The bar diagram plots showing the RMS amplitudes of the Zernike modes detected in the case of centered Gaussian using the (ii)(a) conventional and (iii)(a) proposed GAWS, whereas the bar plots in the case of off-centered Gaussian using the (ii)(b) conventional and (iii)(b) proposed GAWS, respectively, are illustrated. The axis labels appearing in all the images have the unit of radian and the estimated phase profiles using the detected Zernike mode amplitudes are shown in the inset of the respective bar plots.

4. CONCLUSION

In conclusion, an improved GAWS is proposed which is capable of varying the duty cycle of each grating element by changing the transmittance function of the 2D binary diffraction grating array. This is followed by implementation of random binarisation to decrease the contribution from unwanted higher order spots. The working of the proposed GAWS to generate an array of uniform intensity +1 order spots, for different illumination intensity profiles is demonstrated through simulation. The results clearly show that the proposed GAWS is more effective in accurately estimating the incident wavefront when compared to the conventional GAWS, in the presence of non-uniform intensity of the +1 order spots.

ACKNOWLEDGMENTS

Author would like to acknowledge the facilities provided by University of Oxford to carry out the simulation work presented here.

REFERENCES

- [1] W. H. Southwell, "Wave-front estimation from wave-front slope measurements," *J. Opt. Soc. Am.* **70**, 998–1006 (1980).
- [2] B. Pathak and B. R. Boruah, "Improved wavefront reconstruction algorithm for Shack–Hartmann type wavefront sensors," *J. Opt.* **16**, 055403 (2014).
- [3] B. Pathak and B. R. Boruah, "Improvement in error propagation in the Shack–Hartmann-type zonal wavefront sensors," *J. Opt. Soc. Am. A* **34**, 2194–2202 (2017).
- [4] B. R. Boruah, "Zonal wavefront sensing using an array of gratings," *Opt. Lett.* **35**, 202–204 (2010).
- [5] B. Pathak, "Development of a zonal wavefront sensor with enhanced performance using a reconfigurable array of binary diffraction gratings," PhD Thesis, IIT Guwahati Chapter **3**, (2017).
- [6] B. Pathak, A. Das, and B. R. Boruah, "High-speed zonal wavefront sensing," *Proc. SPIE* **8557**, 85570A (2012).
- [7] B. R. Boruah and A. Das, "Zonal wavefront sensor with reduced number of rows in the detector array," *Appl. Opt.* **50**, 3598–3603 (2011).
- [8] B. Pathak and B. R. Boruah, "Zonal wavefront sensing with enhanced spatial resolution," *Opt. Lett.* **41**, 5600–5603 (2016).
- [9] B. Pathak and B. R. Boruah, "A zonal wavefront sensor with multiple detector planes," *J. Opt.* **20**, 035604 (2018).
- [10] G. Cao and X. Yu, "Accuracy analysis of a Hartmann-Shack wavefront sensor operated with a faint object," *Opt. Eng.* **33**, 2331–2336 (1994).
- [11] S. Thomas, T. Fusco, A. Tokovinin, M. Nicolle, V. Michau, and G. Rousset, "Comparison of centroid computation algorithms in a Shack–Hartmann sensor," *Mon. Not. R. Astron. Soc* **371**, 323–336 (2006).
- [12] W. Zou and J. P. Rolland, "Quantifications of error propagation in slope-based wavefront estimations," *J. Opt. Soc. Am. A* **23**, 2629–2638 (2006).
- [13] T. Endo, Y. Miwa, J. Suzuki, and T. Ando, "Improving techniques for Shack-Hartmann wavefront sensing: dynamic-range and frame rate," *The Advanced Maui Optical and Space Surveillance Technologies Conference*, 964–973 (2018).
- [14] C. Baranec and R. Dekany, "Study of a MEMS-based Shack-Hartmann wavefront sensor with adjustable pupil sampling for astronomical adaptive optics," *Appl. Opt.* **47**, 5155–5162 (2008).
- [15] X. Ma, J. Mu, C. Rao, J. Yang, X. Rao, and Y. Tian, "Extension of the modal wave-front reconstruction algorithm to non-uniform illumination," *Opt. Express* **22**, 15589–15598 (2014).
- [16] B. Vohnsen, A. Carmichael, N. Sharmin, S. Qaysi, and D. Valente, "Volumetric integration model of the Stiles-Crawford effect of the first kind and its experimental verification," *J. Vis.* **17**, 18 (2017).
- [17] S. Marcos, L. D. Santana, L. Llorente, and C. Dainty, "Ocular aberrations with ray tracing and Shack–Hartmann wave-front sensors: Does polarization play a role?," *J. Opt. Soc. Am. A* **19**, 1063–1072 (2002).
- [18] T. Fujii, J. Kougo, Y. Mizuno, H. Ooki, and M. Hamatani, "Portable phase measuring interferometer using Shack-Hartmann method," *Proc. SPIE* **5038**, 726–732 (2003).

- [19] N. Kumar, A. Khare and B. R. Boruah, "An ex-situ surface profile measurement scheme using a zonal wavefront sensor with simultaneous presence of reference and test wavefronts," *Proc. SPIE* **11287**, 1128719 (2020).
- [20] B. Pathak, "Improved wavefront estimation accuracy in a programmable grating array based wavefront sensor," *J. Opt.* **23**, 045604 (2021).
- [21] J. E. Harvey and R. N. Pfisterer, "Understanding diffraction grating behavior: including conical diffraction and Rayleigh anomalies from transmission gratings," *Opt. Eng.* **58**, 087105 (2019).
- [22] V. N. Mahajan, "Zernike circle polynomials and optical aberrations of systems with circular pupils," *Appl. Opt.* **33**, 8121–8124 (1994).
- [23] A. Das and B. R. Boruah, "Point Scanning Microscope with Adaptive Illumination Beam Intensity," *AIP Conf Proc.* **1391**, 324–326 (2011).
- [24] C. Maurer, A. Schwaighofer, A. Jesacher, S. Bernet, and M. R. Marte, "Suppression of undesired diffraction orders of binary phase holograms," *Appl. Opt.* **47**, 3994–3998 (2008).
- [25] B. R. Boruah, G. D. Love, and M. A. A. Neil, "Interferometry using binary holograms without high order diffraction effects," *Opt. Lett.* **36**, 2357–2359 (2011).
- [26] M. A. A. Neil, M. J. Booth, and T. Wilson, "Dynamic wave-front generation for the characterization and testing of optical systems," *Opt. Lett.* **23**, 1849–1851 (1998).
- [27] B. R. Boruah, "Dynamic manipulation of a laser beam using a liquid crystal spatial light modulator," *Am. J. Phys.* **77**, 331–336 (2009).